

# Microstructural Evolution and Phase Transformation in Laser Cladding of Cr and Mo Powder on Grey Cast Iron: Mixture Design of Experiment (DOE)

Abd Rahman Zulhishamuddin<sup>a,\*</sup>, Reza Mohamed Suffian<sup>a</sup>, Syarifah Nur Aqida<sup>a,b</sup>,

Maarof Mohd Rashidi<sup>a</sup>

<sup>a</sup>Faculty of Mechanical Engineering, Universiti Malaysia Pahang, 26600, Pekan Pahang, Malaysia

<sup>b</sup>Automotive Engineering Centre, Universiti Malaysia Pahang, 26600, Pekan Pahang, Malaysia

Received: July 27, 2016; Revised: March 09, 2017; Accepted: October 18, 2017

Laser cladding on grey cast iron at high power processing was investigated for microstructural evolution and phase transformation to enhance surface properties. Cladding was designed using a mixture of DOE with peak power (Pp) and pulse repetition frequency (PRF), and a mixture component of Cr and Mo ratio as factors. Microstructural findings indicated absolute elimination of graphite phase from the clad zone, in conjunction with particles evolution occurrence. Meanwhile, Cr, Mo and Fe phases were detected on the clad surface, along with M-C carbide, retained austenite and MoFe formation. The clad surface with addition of Mo exhibited a high hardness value of 945.5 HV<sub>0.1</sub> due to carbide formation. As a result of high peak power penetration into substrate surface, the depth range of clad zone was 53 to 131 μm. From the optimisation, the highest desirability is 82.3 %. Cladding with molybdenum powder addition was found to have produced minimum surface roughness, maximum depth and hardness of 9.14 μm, 110 μm and 891.1 HV<sub>0.1</sub>, respectively.

**Keywords:** Graphite, grey cast iron, laser cladding.

## 1. Introduction

Recent advances in materials design emphasise or focus on sustainability and low cost consumption. Conventional material, such as grey cast iron, is among the cheapest and common engineering materials with a wide range of applications in automotive components such as break disc and cylinder liner. Previous reports from the industry and a number of research have shown that these automotive parts usually experience certain defects such as wear, corrosion and thermal wear<sup>1</sup>. The operational conditions of these parts include elevated temperature, high pressure and sliding friction, which contribute to multifaceted, high-stress condition<sup>2</sup>. Meanwhile, failure of the components made of grey cast iron occurred near-surface graphite phase which acted as a source of crack nucleation under impact condition and caused crack growth. In automotive application, cylinder liner of engines experiences high friction at an elevated temperature that requires such properties to prevent crack and increase the life of cylinder liner. In long-cycle operation, high wear rate leads to corrosion and produces sulphur in the fuel during operation<sup>3</sup>. Therefore, elimination of graphite phase near the surface is an option. With the presence of hard phase on the surface, corrosion and wear can be avoided<sup>4</sup>.

Laser cladding is a process where the added material is deposited onto the substrate with the purpose to improve the properties of the substrate. This process can be achieved by using either laser beam or arc as the heat source to melt

the added material during deposition onto the surface of the substrate. In laser cladding, addition of fine particles like Cr and Mo on the substrate surface resulted in enhanced strength, hardness and wear resistance<sup>5,6</sup>. A previous report showed that modifying surface using tungsten inert gas (TIG) in cast iron surface alloyed with chromium and molybdenum formed the structure of cementite, martensite, as well as retained austenite and primary carbides structure of (Fe,Cr)<sub>7</sub>C<sub>3</sub> and (Fe,Mo)<sub>3</sub>C<sub>5</sub>. As a result, the alloyed surfaces have higher hardness compared to the melting surface because of the carbide formation. Though a lot of works have been conducted on laser cladding of grey cast iron to enhance the hardness and wear resistance using carbon and Fe-based powder<sup>7,8</sup>, there is limited research conducted on laser cladding on grey cast iron surfaced with chromium and molybdenum powder since considerable free carbon, in the form of graphite flakes, is present and laser surface modification on cast iron is challenging<sup>9</sup>. Thus, this research aims to study surface modification of grey cast iron by pre-placing chromium, molybdenum and mixture between them on the grey cast iron using laser cladding. This study also aims to optimise laser processing to enhance cylinder liner life and prevent premature failure of friction due to high temperature.

## 2. Materials and Methods

As-received grey cast iron was cut into samples of 40 mm diameter and 10 mm thickness. The chemical

\*e-mail: [zulhishamuddin@yahoo.com](mailto:zulhishamuddin@yahoo.com)

composition of the as-received grey cast iron is shown in Table 1, whereas Figure 1 shows the microstructure of the as-received grey cast iron. The structure shows that graphite lamella is surrounded with  $\alpha$ -ferrite and pearlite. The average hardness for this material is 278.5 HV<sub>0.1</sub>. Cr and Mo powders of 99.9 % purity, with the particle size range of 71.9 to 130  $\mu\text{m}$  and 0.969 to 9.62  $\mu\text{m}$  respectively, were used. These powders were mixed with a bonding agent called sodium silicate prior to pre-placement on grey cast iron substrate surface. The pre-placed powders were dried in a furnace at the temperature of 200°C for 2 h. This technique is to bind the powders and prevent them from being dispersed during laser processing<sup>10,7</sup>. The thickness of the pre-placed powder layer was in the range of 0.3 to 0.7 mm as the alloying component had the maximum penetration amount in the thickness of coating<sup>11</sup>.

A comprehensive experiment that combines a mixture of components with process factor was used to design laser cladding of grey cast iron with the addition of Cr and Mo particles. The combined mixture components design of experiment was developed at two numerical factor and mixture component at two levels to yield 12 parameter settings. The mixture components were Cr and Mo, while peak power ( $P_p$ ) and pulse repetition frequency (PRF) were the process factors. Three responses were depth of molten zone, surface roughness and hardness. The outcome parameters from the setting were pulse energy ( $E_p$ ), residence time ( $T_R$ ) and irradiance ( $I$ ). Setting the parameter at different values was found to produce significant amounts of energy and irradiance to melt and clad the sample at laser spot size of 1 mm. The design was optimised for minimum surface roughness and maximum surface depth and hardness.

Laser processing was conducted using JK300HPS Nd:YAG twin lamp laser source pulse TEM<sub>00</sub> mode, 50 W average power, 1064 nm wavelength at the laser spot size of 1 mm. The laser cladding parameters were peak power in range of 800 to 1200 W, pulse repetition frequency in range of 80 to 90 Hz and the scan speed in the range of 2.4 to 21.6  $\text{mm}\cdot\text{s}^{-1}$ . During the laser processing, surface of the sample was heated up from room temperature to its melting temperature. Meanwhile, the cooling period ( $t_{\text{cooling}}$ ) of the sample was determined from the 'off' state duration of the laser pulse (see Equation 1). Hence, the cooling rate ( $C_R$ ) can be calculated as per Equation 2.

$$t_{\text{cooling}} = \frac{1}{\text{PRF}} - T_R \quad (1)$$

$$C_R = \frac{\Delta T}{t_{\text{cooling}}} \quad (2)$$

**Table 1.** Chemical composition for as-received grey cast iron.

Material	C	Si	Mn	P	S	Fe
Grey cast iron	3.55	1.58	0.76	0.09	0.08	Bal.

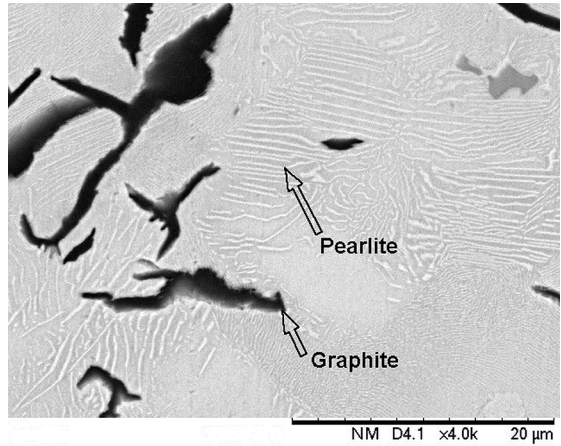


**Figure 1.** Microstructure as-received of grey cast iron at 500 $\times$  magnification.

Where,  $\Delta T$  is temperature deviation from room temperature to the melting temperature. The parameter setting and outcome parameters are summarised in Table 2. The sample was placed on the table with linear movement translated by CNC moving control system. In order to prevent oxidation, laser processing was assisted by argon gas in constant flow at 10  $\text{L}\cdot\text{min}^{-1}$ .

Metallographic study was carried out using IM7000 Series Inverted Optical microscopes with Progress Capture 28.8 Jenoptik Optical System image analyser software and scanning electron microscopes (SEM). The modified surface roughness was determined using the 2D stylus profilometer model Mitutoyo SJ-410 series. X-ray diffractometer model Rigaku Miniflex with Cu  $K\alpha$  was generated at 30 kV and current of 15 mA, while a scanning range of 3° to 80° was used to analyse presence of the phase in the modified surface. Meanwhile, the PDXL analysis software was used to identify the phase from the x-ray diffraction result. The range of penetration depth ( $\tau_{1/e}$ ) for some substances in Cu  $K\alpha$  is 0.1 to 10  $\mu\text{m}$ , which is in the range of a typical layer thickness<sup>12</sup>. Hardness properties were measured using MMT Matsuzawa Vickers Hardness tester with 100 gf load. The experimental results were statistically analysed by using the ANOVA approach to establish the relationship between the factors and responses.

### 3. Results and Discussion

The metallographic study revealed a clad layer formation on the grey cast iron substrate, as shown in Figure 2. The micrographs of modified sample cross section in Figure 2 indicate the presence of clad zone, interface zone and substrate material. The clad zone depth is 127  $\mu\text{m}$ , 131  $\mu\text{m}$  and 96

**Table 2.** Parameter settings for laser surface cladding of grey cast iron.

Num.	A:	B:	Input parameter					Outcome	
	Cr	Mo	Pp	PRF	Pave	V	Ep	T <sub>R</sub>	I
	%	%	W	Hz	W	mm/s	J	s	W/mm <sup>2</sup>
1	100	0	800	80		19.2	0.63	0.0033	
2	100	0	800	90		21.6	0.56	0.0029	
3	100	0	1200	80		19.2	0.63	0.0022	
4	100	0	1200	90		21.6	0.56	0.0019	
5	0	100	800	80		19.2	0.63	0.0033	
6	0	100	800	90	50	21.6	0.56	0.0029	
7	0	100	1200	80		19.2	0.63	0.0022	15.28
8	0	100	1200	90		21.6	0.56	0.0019	
9	50	50	800	80		19.2	0.63	0.0033	
10	50	50	800	90		21.6	0.56	0.0029	
11	50	50	1200	80		19.2	0.63	0.0022	
12	50	50	1200	90		21.6	0.56	0.0019	

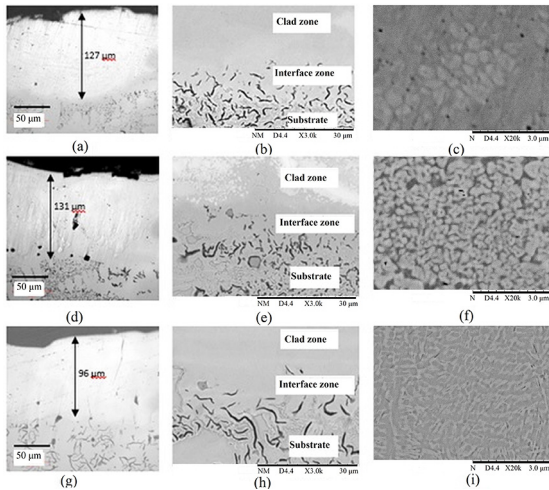


**Figure 2.** Micrograph of laser cladding grey cast iron section with addition of Cr powder (a) - (c), Mo powder (d) - (f) and Cr-Mo mixture powder (g) - (i).

μm, as illustrated in Figures 2(a), (d) and (g). The clad zone with chromium, molybdenum and mixture particle addition formed a graphite-free layer, as shown in the micrographs (b) (e) and (h) of Figure 2. In addition, elimination of graphite was also observed by other researchers when the surface of cast iron was modified through laser alloying processes<sup>6,13,14</sup>. Full dissolution of graphite at alloy zone was due to the high cooling rate during solidification. The microstructure clad zone for Cr, Mo and Cr-Mo mixture is shown in the micrographs (c) (f) and (i) of Figure 2, respectively. In the clad zone of Cr and Mo, an enormous amount of bright particles was randomly dispersed at or near the boundaries of the dendrite, while occasionally interspersed black particles were observed in the matrix. These results indicate that the melted Cr and Mo might enter the metastable miscibility gap and liquid phase separation that had taken place due to rapid solidification.

Moreover, uniform deposition can be observed in Cr-Mo added after etching, while the element of substrate had diffused to the modified layer. Hence, it is proven on carbon diffusion where the graphite is eliminated. At a moderate cooling rate if  $< 5000 \text{ Ks}^{-1}$ , the main microstructure structure is that of an interconnected network of primary dendritic with interdendritic eutectic<sup>15</sup>. However, laser cladding with Cr and Mo at the high cooling rates in the range of  $21.2 \times 10^5 \text{ Ks}^{-1}$  to  $3.52 \times 10^5 \text{ Ks}^{-1}$  caused the microstructure to develop a lath type morphology with a refinement of the structure scale of the laths, together with bright spheroidal particles which were evident at the highest cooling rate. According to the solidification theory, the dendritic characteristic length is inversely proportional to the cooling rate, and hence, laser cladding with added Cr-Mo has shown smaller than addition of others. The bigger particle of chromium powder formed bigger sizes of bright particles compared to the small particle powder of molybdenum. The combination of chromium and molybdenum powder showed the formation of small dendrite structure with fine particles. The different sizes of the particles in the clad zone are due to the change of laser power varied surface heating and cooling rate<sup>16</sup>.

Figure 3 shows the particle analysis of clad zone, in modified samples with addition of Cr, Mo and Cr-Mo mixture powder. It shows bright particles structure with the average size of 123 nm formed in the clad zone. However, the clad surface with molybdenum produced much smaller particle size, which is in average of 57 nm. The clad zone with a mixture of 50 % Cr and 50 % Mo shows that the particles structure is finer and homogenous in the size of 32 nm. Smaller dendrites, together with smaller structure of bright particles, contribute to greater hardness of the clad layer<sup>17</sup>. These sizes produced different results because of the particle sizes used for cladding. The melting point for pure chromium is lower than molybdenum. However, the

different of the powder size elements is high, which is at 92.6%. It is a known fact that smaller particle sizes tend to be heated and accelerated more quickly at a higher temperature and velocity<sup>18</sup>. Moreover, surface layers and substrate were bonded through the interface zone that exhibited excellent metallurgical bonding generation.

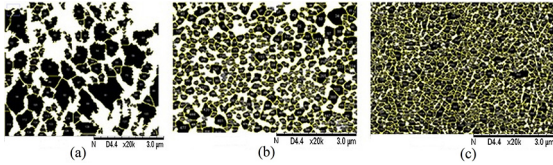


**Figure 3.** Analyze particle in clad zone for (a) chromium, (b) molybdenum and (c) mixture.

In Figure 4(a), the as-received grey cast iron sample consists of ferrite ( $\alpha$ -Fe), cementite ( $\text{Fe}_3\text{C}$ ) and graphite phases. The  $\alpha$ -Fe phase intensity reduced to 34.2 %, 64.3 % and 60.5 % in respective to the Cr, Mo and Cr-Mo cladding samples. The graphite phases were absent in all the cladding layers patterns shown in Figures 4(b)-(d). Meanwhile, the carbide phases were only detected in Mo and Cr-Mo added cladding layer, which are  $\text{M}_2\text{C}$ ,  $\text{M}_{23}\text{C}_6$  and  $\text{M}_3\text{C}_2$ . In Figure 4(c), apart from the carbide phases, the cladding layer also comprised retained austenite.

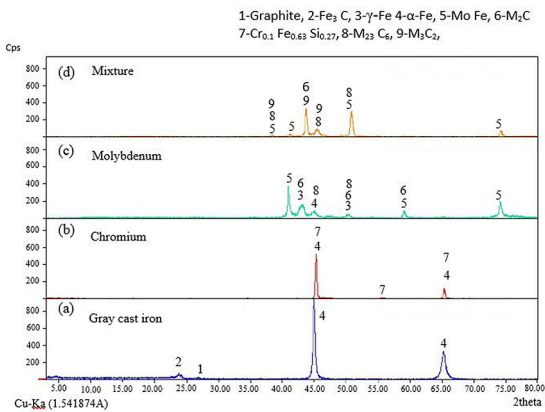


**Figure 4.** X-ray diffraction pattern for (a) grey cast iron substrate, (b) Cr-added clad, (c) Mo-added clad and (d) Cr-Mo mixture clad zone.

A decrease in the  $\alpha$ -Fe phase intensity in the cladding sample was due to the phase transformation at high heating and cooling rates. In the cladding zone, no graphite was observed because at the high temperature of molten pool, the graphite is diffused to the substrate region during the remelting processing<sup>7</sup>. However, in the interface zone, some graphite phases remained due to the reduced heat input as the energy travelled into the surface. The carbide formation phase in the cladding layer was due to the high concentration of Cr and Mo particles, along with the high carbon composition of grey cast iron substrate. Although both Cr and Mo are carbide formers, Mo particles in the cladding surface produced slight

carbide phase content compared to the Cr-Mo particles, where the amount of carbide phase for the added Mo clad sample was 21.2 % for  $\text{M}_{23}\text{C}_6$  and 32.3 % for  $\text{M}_2\text{C}$ , while for the added Cr-Mo clad sample was 29.9 % for  $\text{M}_{23}\text{C}_6$  and 24 % for  $\text{M}_3\text{C}_2$ . The  $\text{M}_{23}\text{C}_6$  carbides could be observed in both the added particles, which are associated with slower growth rates and longer times available for redistribution of carbon and carbide forming elements both in the liquid and solid phases<sup>19</sup>. In the cladding layer with the addition of Cr particles and given that there was a bigger particles size range, the rapid cooling during cladding was inadequate to allow carbide precipitation in the cladding zone. According to the Fe-C phase diagram, pearlite in substrate begins to decompose into ferrite and cementite as the temperature exceeds the eutectoid point, whereas pearlite transforms into austenite. As the temperature continuously increases, the primitive ferrite is converted into austenite, with some carbon elements decomposing into austenite. However, because of the rapid cooling rate, some austenite cannot be converted completely and thus turn into residual austenite<sup>20</sup>.

In comparison with the Cr added sample, the Mo and Cr-Mo added samples exhibited hardness properties of 945.5  $\text{HV}_{0.1}$ . Thus, lower hardness of 496.15  $\text{HV}_{0.1}$  was measured in the Cr added sample. Parallel with the XRD results, the formation of carbides in Mo and Cr-Mo added clad surface increased the hardness properties. In agreement with a previous work, the formation of carbide in the clad zone contributed to the increase of hardness<sup>21</sup>. Relatively, the dual increase of hardness properties in the Cr-added clad from its substrate was because of grain formation. Meanwhile, rapid quenching of  $3.52 \times 10^5 \text{ K s}^{-1}$  and presence of particles during solidification obstructed atom settlement, thus resulting in grain formation in cast iron.

Table 3 shows the range of layer depth of the clad zone, surface roughness and subsurface hardness of the samples at 1 mm laser spot size. The highest clad layer thickness is 131  $\mu\text{m}$  for the Mo-added sample, while the lowest clad layer is 7.72  $\mu\text{m}$  for the Cr-Mo mixture sample. The minimum range of surface roughness was achieved in the Cr-added sample at 8.01 to 13.10  $\mu\text{m}$ . The sample with Cr-Mo mixture clad developed a surface roughness range of 7.72 -13.11  $\mu\text{m}$ . A higher surface roughness ranging between 10.50  $\mu\text{m}$  and 18.96  $\mu\text{m}$  was obtained at the clad with molybdenum powder. The increment of the sample clad depth with molybdenum was due to the increased peak power and decreased traverse speed. Similar results were found in the laser surface alloying of chromium on austenitic stainless steel<sup>22</sup>. Furthermore, the high thermal conductivity of grey cast iron allows a high laser energy of 0.63 J to penetrate deeper at 131  $\mu\text{m}$  into the substrate surface with the Mo-added powder. However, the high energy caused rough surface finish as previously reported<sup>23</sup>. The surface of clad layer required post-processing such as grinding and polishing at high precision within

**Table 3.** Surface roughness, depth and hardness of clad zone laser surface cladding range spot sizes 1 mm.

Num.	A:	B:	Input parameter			Outcome parameter			Ra (μm)	Depth (μm)	Hardness HV <sub>0.1</sub>
	Cr	Mo	P <sub>p</sub>	PRF	E <sub>p</sub>	T <sub>R</sub>	I	τ			
	%	%	W	Hz	J	ms	W/mm <sup>2</sup>	ms			
1	100	0	800	80	0.63	3.3		0.78	13.10	0.127	566.30
2	100	0	800	90	0.56	2.9		0.69	10.60	0.122	460.35
3	100	0	1200	80	0.63	2.2		0.52	13.08	0.098	496.15
4	100	0	1200	90	0.56	1.9		0.46	11.80	0.101	460.65
5	0	100	800	80	0.63	3.3		0.78	18.96	0.067	938.10
6	0	100	800	90	0.56	2.9	15.28	0.69	11.20	0.053	991.05
7	0	100	1200	80	0.63	2.2		0.52	15.45	0.131	995.50
8	0	100	1200	90	0.56	1.9		0.46	13.04	0.095	911.05
9	50	50	800	80	0.63	3.3		0.78	7.72	0.096	875.05
10	50	50	800	90	0.56	2.9		0.69	7.00	0.054	922.10
11	50	50	1200	80	0.63	2.2		0.52	8.38	0.093	981.85
12	50	50	1200	90	0.56	1.9		0.46	7.50	0.083	998.25

depth range and low surface temperature to avoid material properties reduction<sup>22</sup>.

### 3.1. Design optimization

The statistical analysis for hardness response indicates a significant model for the selected range of laser parameters and powder mixture. Table 4 shows the ANOVA analysis for hardness response. Based on the data, model F-value of less than 0.05 shows that the model is significant. All the factors were found to be significant with non-significant lack of fit.

Optimisation analysis was conducted to design an experiment within the given range of P<sub>p</sub>, PRF and percentages of chromium and molybdenum, with the aim to minimise surface roughness and maximise depth of clad zone and hardness. The highest and lowest desirability were represented by 1 and 0 value, respectively. Figure 5 shows the contour plot of predicted for higher desirability for spot size 1 mm. The optimisation analysis produced a desirability range of 77% to 82.3%. High cladding molybdenum, with high peak power and pulse repetition rate, produced minimum surface roughness, maximum depth and hardness at 9.14 μm, 110 μm and 891.1 HV<sub>0.1</sub>, respectively. P<sub>p</sub> and PRF are significant factors to optimise the surface of grey cast iron through laser processes.

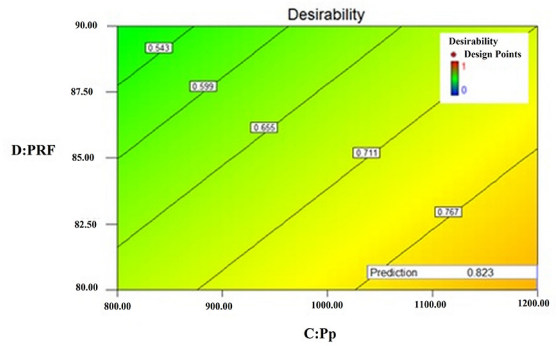


**Figure 5.** Contour plot of process optimization for laser surface cladding of grey cast iron at 1 mm laser spot size.

## 4. Conclusion

Laser surface cladding using Nd:YAG laser system was conducted based on the combination of mixture components design of experiment (DoE) for grey cast iron. From the metallographic study, the graphite phase was eliminated from the clad zone in all the samples processed with addition of Cr, Mo and Cr-Mo powder mixture. In the clad zone, a new hard face layer structure had formed in the dendritic structure. The formation of small dendritic and spheroidal

**Table 4.** ANOVA analysis of hardness response for laser cladding of grey cast iron with Cr and Mo powders addition.

Spot size (mm)	Source	Sum of squares	df	Mean square	F value	p-value Prob>F	
1.0	Model	390700	2	195300	78.56	< 0.0001	significant
	Linear Mixture	341200	1	341200	137.24	<0.0001	
	AB	49445	1	49445	19.89	0.0016	
	Residual	22378	9	2486			
	Cor Total	413100	11				

particles in the clad zone is due to rapid solidification and presence of the powders. The formation of carbide was detected in the Mo and Cr-Mo powder added samples, whereas in the Cr added sample, carbide phase was absent. High concentrations of chromium and molybdenum in the clad zone with high carbon composition in substrate had caused the formation. However, the high cooling rate in the chromium added sample might have caused the carbide to have inadequate time to precipitate in the clad zone. The formation of carbide phase is an advantage for surface performance with high hardness, high temperature wear resistance and also corrosion resistance, which are parallel with the findings for hardness properties characterisation. The samples with Mo and Cr-Mo powder mixture increased the hardness of grey cast iron surface up to 945.5 HV<sub>0.1</sub> due to the presence of fine grains. Increment in the subsurface hardness measured in the clad zone was up to three times of its substrate. The highest layer depth was measured in the samples processed at alloy molybdenum, whereby the higher energy settings contributed to the high alloy layer depth. Nonetheless, surface roughness was also high because if the high energy on laser beam. Therefore, optimization of laser parameters for minimum surface roughness and maximum hardness and alloy layer depth has shown the highest desirability factor of 0.823. These findings signify the preferred parameters for the laser surface alloy of grey cast iron for enhanced surface properties and prolonged cylinder liner life.

## 5. Acknowledgements

The authors would like to acknowledge the financial support by Universiti Malaysia Pahang (Grant No.: RDU 160399) and laser facilities provided by Precision Machining Research Centre of Universiti Tun Hussein Onn, Malaysia.

## 6. References

- Polak A, Grzybek J. The mechanism of changes in the surface layer of grey cast iron automotive brake disc. *Material Research*. 2005;8(4):475-479.
- Ghasemi R, Elmquist L. The relationship between flake graphite orientation, smearing effect, and closing tendency under abrasive wear conditions. *Wear*. 2014;317(1-2):153-162.
- Jeong BY, Kim MH. Corrosion characteristics of duplex surface-treated spheroidal graphite cast iron. *Surface and Coatings Technology*. 2001;141(2-3):262-268.
- Nadel J, Eyre TS. Cylinder liner wear in low speed diesel engines. *Tribology International*. 1978;11(5):267-271.
- Amirsadeghi A, Sohi MH. Comparison of the influence of molybdenum and chromium TIG surface alloying on the microstructure, hardness and wear resistance of ADI. *Journal of Materials Processing Technology*. 2008;201(1-3):673-677.
- Tong X, Zhou H, Ren L, Zhang Z, Cui R, Zhang W. Thermal fatigue characteristics of gray cast iron with non-smooth surface treated by laser alloying of Cr powder. *Surface and Coatings Technology*. 2008;202(12):2527-2534.
- Chen Z, Zhou T, Zhao R, Zhang H, Lu S, Yang W, et al. Improved fatigue wear resistance of grey cast iron by localized laser carburizing. *Materials Science and Engineering: A*. 2015;644:1-9.
- Yi P, Xu P, Fan C, Li C, Shi Y. The Effect of Dynamic Local Self-Preheating in Laser Cladding on Grey Cast Iron. *Journal of Mechanical Engineering*. 2015;61(1):43-52.
- Hussein NIS, Kamarul SR, Ayof MN. Preliminary study of on cladding process on grey cast iron substrate. *International Journal of Research in Engineering Technology*. 2013;2(11):5-11.
- Sohi MH, Ebrahimi M, Ghasemi HM, Shahripour A. Microstructural study of surface melted and chromium surface alloyed ductile iron. *Applied Surface Science*. 2012;258(19):7348-7353.
- Chen Z, Meng C, Dong J, Zhou T, Tong X, Zhou H. The comparative study of W/Cr addition in Fe-base by laser surface alloying on fatigue wear resistance of GCI. *Surface and Coatings Technology*. 2016;286:25-35.
- Birkholz M. Principles of X-Ray Diffraction. In: Birkholz M. *Thin Film Analysis by X-Ray Scattering*. Weinheim: Wiley-VCH Verlag; 2006. p. 1-40.
- Zhong M, Liu W, Zhang H. Corrosion and wear resistance characteristics of NiCr coating by laser alloying with powder feeding on grey iron liner. *Wear*. 2006;260(11-12):1349-1355.
- Yang X, Zhang Z, Wang J, Ren L. Investigation of nanomechanical properties and thermal fatigue resistance of grey cast iron processed by laser alloying. *Journal of Alloys and Compounds*. 2015;626:260-263.
- Oloyede O, Cochrane RF, Mullis AM. Effect of rapid solidification on the microstructure and microhardness of BS1452 grade 250 hypoeutectic grey cast iron. *Journal of Alloys and Compounds*. 2017;707:347-350.
- Fauzun F, Aqida SN, bin Wahab S. Laser Surface Modification of AISI 1025 Low Carbon Steel using Pulsed Nd:YAG Laser for Enhanced Surface Properties. *Key Engineering Materials*. 2013;554-557:596-602.
- Norhafzan B, Aqida SN, Chikarakara E, Brabazon D. Surface modification of AISI H13 tool steel by laser cladding with NiTi powder. *Applied Physics A*. 2016;122:384.
- Chivavibul P, Watanabe M, Kuroda S, Kawakita J, Komatsu M, Sato K, et al. Effect of Powder Characteristics on Properties of Warm-Sprayed WC-Co Coatings. *Journal of Thermal Spray Technology*. 2010;19(1-2):81-88.
- Wieczerzak K, Bala P, Stepień M, Cios G, Koziel T. Formation of eutectic carbides in Fe-Cr-Mo-C alloy during non-equilibrium crystallization. *Materials & Design*. 2016;94:61-68.
- Yi P, Xu P, Fan C, Yang G, Liu D, Shi Y. Microstructure Formation and Fracturing Characteristics of Grey Cast Iron Repaired Using Laser. *The Scientific World Journal*. 2014;2014:541569.

21. Chung RJ, Tang X, Li DY, Hinckley B, Dolman K. Microstructure refinement of hypereutectic high Cr cast irons using hard carbide-forming elements for improved wear resistance. *Wear*. 2013;301(1-2):695-706.
22. Brytan Z, Bonek M, Dobrzański LA. Microstructure and properties of laser surface alloyed PM austenitic stainless steel. *Journal of Achievement in Materials and Manufacturing Engineering*. 2010;40(1):70-78.
23. Hwang JH, Kim DY, Youn JG, Lee YS. Laser surface hardening of grey cast iron used for piston ring. *Journal of Materials Engineering and Performance*. 2002;11(3):294-300.